Aluminosilicate glass waveguide platform for connecting optical fiber sensors embedded in composite materials.

Thibault Juwet*[a,b], Eli Voet[a], Jeroen Missinne[b]
[a]Com&Sens, Begoniastraat 5, 9000 Gent, BE; [b]Centre for Microsystems Technology (CMST), Ghent University - Imec, Technologiepark 126, 9052 Zwijnaarde, BE

ABSTRACT

In this paper, the building blocks for a smart glass connector platform are presented. The connector is meant to connect optical fibers, which cannot be connected using conventional connector or splicing technology, e.g. optical sensing fibers embedded in composite structures for structural health monitoring purposes. We are setting up a technology platform using aluminosilicate glass substrates as interposer between 2 optical fibers that need to be connected. Using femtosecond laser technology, this interposer can be equipped with basic building blocks such as low-loss intermediate single mode waveguides, couplers and Bragg grating sensors. To this end, femtosecond laser-written waveguides are inscribed in aluminosilicate glass (Xensation® Cover float glass) and the laser parameters are optimized. Waveguides with estimated propagation losses of 0.65 dB/cm are obtained and are subsequently used to make couplers in glass. These couplers can be tuned in coupling ratio between 87:13 and 15:85 by varying the coupling length from 1 to 4.5 mm at a pitch of 17 µm. In addition, fs-laser written Bragg gratings were manufactured, with the goal to add monitoring capabilities to the interposer. These were realized by modulating the fs-laser pulse train and as such a reflectivity up to 5.9% was achieved in the C-band for 23 mm long Bragg gratings. When properly designed, these can be made compatible with standard read out equipment for fiber Bragg gratings (FBGs).

Keywords: Aluminosilicate glass, Bragg gratings, couplers, connector, femtosecond laser, optical fiber sensing, waveguides, waveguide coupling

1. INTRODUCTION

Optical fiber sensors are used in a variety of applications and different sensing techniques can be used to measure e.g. strain, temperature, refractive index changes and hydrogen concentration. A common example is the use of optical fibers with Fiber Bragg gratings (FBGs) for in-situ strain and temperature measurements. Such optical fibers can be embedded for example in composite structures [1] or concrete [2] and can be used for structural health monitoring (SHM) [3], monitoring of cracks or debonding in hybrid joints [4], or temperature mapping [5]. Optical fiber sensors can also be used in a variety of environmental sensing applications [6] like pipeline leak monitoring, or monitoring of air, soil and water quality for agriculture purposes. In these, sometimes, harsh environments optical fiber sensors are advantageous due to their resistance to extreme temperatures and high pressures and immunity to electromagnetic interference. Finally, Fiber Bragg gratings are used in medical applications [7] such as for studying joint kinematics or respiratory and heart rate monitoring by integrating the FBGs in wearables or for retinal microsurgery where FBGs are integrated in the tool-tip to enable force monitoring during surgery. As optical fibers do not suffer from electromagnetic interference, they can be used for example for measuring tissue temperature during MRI-guided hyperthermic treatment [8].

To perform these measurements, the embedded optical fiber should be connected to a read-out unit. This can be achieved by either co-integrating the read-out unit in the embedding material/structure [9] or by providing a lead-out optical fiber. While co-integrating the read-out unit is more complex than providing a lead-out optical fiber, the latter also asks for extra attention at the egress point, i.e. the location where the optical fiber leaves the material in which it is embedded (Figure 1). Production processes typically need to be adapted to accommodate the egress point. For example, figure 1 shows the addition of Polytetrafluoroethylene (PTFE) tubing to protect the optical fiber at the egress point. Furthermore, it shows that it is impossible to trim and polish the edges, a typical finishing step when manufacturing composite structures. In addition, the egress point typically forms the weak spot of the optical fiber due to stress concentrations and when the optical fiber breaks at the egress point, it is often impossible to reconnect the optical fiber with conventional splicing techniques.

*thibault.juwet@ugent.be

Optical Fibers and Sensors for Medical Diagnostics, Treatment, and Environmental Applications XXIV, edited by Israel Gannot, Katy Roodenko, Proc. of SPIE Vol. 12835, 128350B
 · 1605-7422 · doi: 10.1117/12.3001914

Therefore, a platform is being developed to facilitate connecting such embedded optical fibers. The proposed idea relies on an intermediate aluminosilicate glass connection piece, equipped with optical features such as low-loss single mode waveguides, couplers and Bragg gratings. As such, the strain in the connector itself or at the glass-glue interface can be monitored or temperature can be monitored for example to perform temperature compensation [10]. These features are inscribed in the glass by means of femtosecond laser writing [11][12][13][14] which allows for 3D processing of the glass. In this paper, the realization, optimization and characterization of this platform's basic buildings blocks are presented.

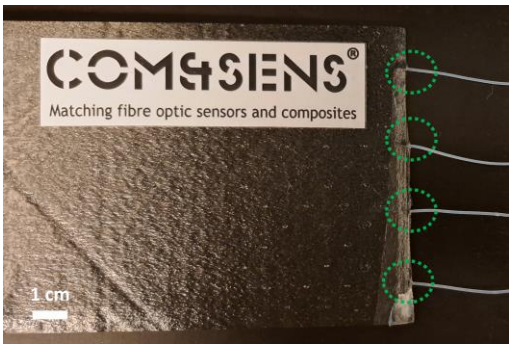

Figure 1. Illustration of the egress point (encircled in green), here with protective PTFE tubing.

2. MATERIALS AND METHODS

2.1 Femtosecond laser writing in aluminosilicate glass

The optical features are inscribed into glass pieces using an ytterbium-doped fiber laser (pulse length <400 fs, repetition rate 500 kHz, and frequency-doubled operating wavelength of 515 nm (Satsuma, Amplitude Systèmes)). Xensation® Cover float glass (thickness of 500 µm) from Scott is used, which was diced into 25x25 mm pieces and mounted on a motorized xy stage in the laser system. The laser beam is focused into the glass using an aspheric lens with numerical aperture 0.55 (Newport 5722-A-H). The polarization of the beam is controlled by passing it through a half-wave plate and a quarter-wave plate. For this work, linear polarization perpendicular to the writing direction is used.

2.2 Optimization and characterization of single mode waveguides

Waveguides were inscribed 100 µm below the surface of the glass with varying writing speed (0.27, 0.5, 1, 5 and 10 mm/s) and pulse energy (100, 125, 150 and 175 nJ), to find the optimal parameter set, i.e. resulting in a minimum insertion loss. For each set of parameters, 5 waveguides were inscribed over the whole length of the glass sample, as shown in figure 2. The edges were subsequently diced off (wafer dicer equipped with diamond blade) and polished (Mecapol P310) to obtain 23 mm long waveguides with optical quality end faces.

The insertion loss was measured using a 1550 nm diode laser (QPhotonics, QDFBLD-1550-20DIL) and power meter (Newport power meter 1930C) with IR photodetector (Newport 818-FA). Two standard SMF-28 fibers were aligned with the waveguide at both sides of the glass sample without the use of index matching fluid. The transmitted power was then recorded and compared with that of a reference measurement (transmission from input fiber to output fiber).

In addition, the mode profiles were measured using a Xenics infrared (IR) camera and the mode field diameters (MFD) were extracted in the y and x directions (using the x, y, z conventions as indicated in Figure 2). A conversion factor (c = 0.352 µm/pixel) from pixels to µm was obtained by calibrating the Xenics IR camera using an FBG sensor fiber, type Draw Tower Grating (DTG) form FBGS (Germany) and SMF-28 optical fiber with known MFDs of 6 µm and 10.4 µm. The measured mode profiles were used to calculate the overlap integral with the expected mode profile in the SMF-28 optical fibers to estimate the coupling loss between fiber and waveguide.

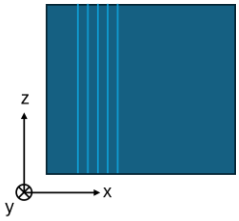

Figure 2. Schematic view of a glass sample with inscribed waveguides and the convention for the x, y and z coordinates used in the paper.

The extracted MFDs were also used to fit the dimensions of the waveguides in a numerical simulation model (finite difference eigenmode, FDE, Lumerical). The waveguide was modelled with an elliptical cross section and a step index refractive index (RI) profile in bulk aluminosilicate glass with a RI of 1.496 at 1550 nm. The short (x) and long (y) axis dimensions and refractive index difference were varied to fit the measured MFD. The RI of the aluminosilicate glass at the target wavelength was obtained by applying Cauchy's equation:

$$n(\lambda) = A + \frac{B}{\lambda^2} \tag{1}$$

And fitting the parameters A (=1.494) and B (=4809) to the given RI at 588, 633 and 780 nm.

2.3 Waveguide to waveguide coupler in glass

The coupler was first simulated using the fitted waveguide model in an eigenmode expansion (EME) simulation in Lumerical to extract the coupling ratio for a certain pitch and coupling length at a wavelength of 1550 nm. The optimal parameters for waveguiding were then used to manufacture couplers with a pitch (center-to-center) of 17 µm with varying coupling length (3 to 17 mm).

For each coupler, one waveguide was inscribed over the whole length of the glass and a second shorter waveguide was inscribed at a 17 µm offset. The length of the second waveguide determined the coupling length, as illustrated in Figure 3a. The end facets were again diced off and polished as described above.

The couplers were characterized by coupling light in the first waveguide and inspecting the spot intensities at the opposite side with the IR camera. The coupling ratio was determined by dividing the maximum intensity of both spots through the sum of both maximum intensities.

The results were verified with a sample with a coupler as shown in Figure 3b. The aim was to obtain a 30:70 coupling ratio between a first straight waveguide, inscribed over the whole length of the sample, and a second waveguide, inscribed starting at 1 mm form the in-coupling side in parallel with a pitch of 17 µm and overlap length of 6 mm, which was subsequently extended under an angle (1°). As such, both waveguides were separated by 300 µm at the out-coupling side. The end facets were again diced off and polished as described above. A schematic overview is shown in Figure 3b. The insertion loss was measured with the same methods as explained in section 2.2.

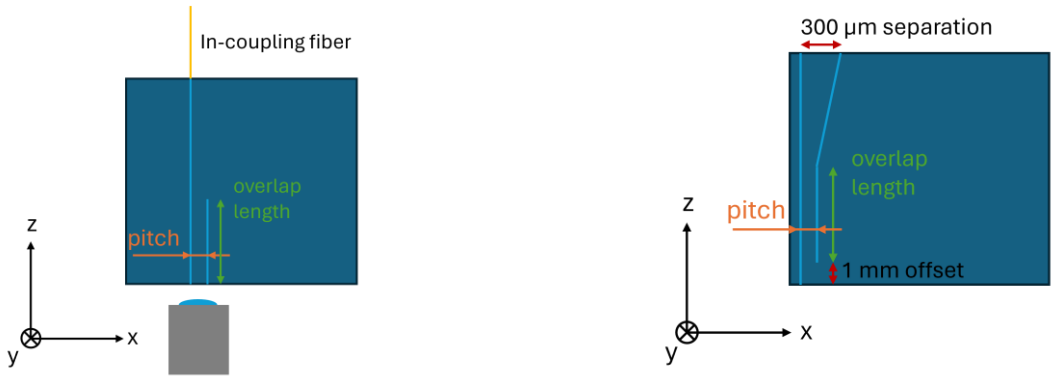

(a) (b)

Figure 3. Figure (a) shows a schematic overview of the coupler fabrication scheme and inspection method. Figure (b) shows a schematic of the coupler with 6 mm overlap length and diverging part to obtain a 30:70 coupling ratio.

2.4 Bragg gratings

First order Bragg gratings at a Bragg wavelength (λ_B) of 1550 nm were inscribed by applying an external modulation to the pulse train emitted by the laser. The pulse energy (300, 500 and 600 nJ), writing speed (0.1, 0.25 , 0.5, 0.75 and 1 mm/s) and duty cycle (10, 25 and 50 %) were varied to find the optimum parameters. The modulation frequency was adapted to the writing speed to ensure the correct grating period Λ = 518 µm ($\lambda_B = 2 \cdot n_e \cdot \Lambda$, with n_e = 1.496). The Bragg grating was inscribed over the whole length of the glass and the end facets were again diced off and polished. Thus 23 mm long Bragg gratings were obtained.

The Bragg gratings were characterized using a broadband diode source (Exalos 1550 nm SLED) connected to port 1 of a circulator and an optical spectrum analyzer (OSA, Agilent 86142B optical spectrometer) connected to port 3 of the circulator. At port 2, an SMF-28 optical fiber was connected which was cleaved and aligned with the glass sample having the Bragg gratings. Index matching fluid was used to avoid unwanted air-glass transition reflections. The absolute reflectivity was calculated (Equation 2) by comparing the measured reflection spectrum with that of the cleaved optical fiber (with tip in air):

$$I_{refl}(\lambda) = 10^{\frac{P_{FBG} - P_{Fres}}{10}} \cdot R_{Fres} \tag{2}$$

Where I_{refl} is the reflectivity, P_{FBG} is the measured power in reflection of the FBG and P_{Fres} the measured reflected power at the cleaved optical fiber tip and R_{Fres} the Fresnel reflection coefficient:

$$R_{Fres}[\%] = \left(\frac{n_{air} - n_{SMF28}}{n_{air} + n_{SMF28}}\right)^2 \cdot 100 = 3.4 \tag{3}$$

With n_{air} and n_{SMF28} the refractive indexes of air and the SMF-28 fiber core equal to 1 and 1.45213, respectively.

3. RESULTS AND DISCUSSION

3.1 Laser-written waveguides

Figure 4 shows the measured insertion losses obtained for the different parameter. The lowest insertions losses were achieved with a writing speed of 5 mm/s with 300 nJ pulse energy. An example of the measured mode profile associated with these parameters is shown in figure 5. All observed profiles were slightly elliptical with quasi gaussian cross sectional profiles in x and y direction. For the optimum parameters, the MFDs in x and y direction were 13.77±0.91 and 15±1.53 µm respectively. The overlap integrals for the measured mode profiles of the waveguides and a standard SMF-28 fiber were calculated and amounted to a mean value of 0.53±0.15 dB. Given the mean total insertion loss of 2.91±0.2dB (= 2x coupling loss, 2x aluminosilicate glass-air interface transition loss and propagation loss in 23 mm long waveguide), the propagation loss can be estimated to be 0.65 dB/cm for the optimum writing parameters.

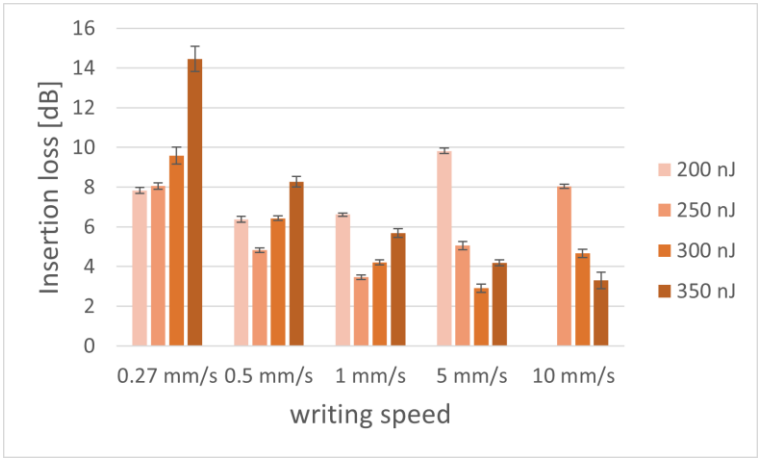

Figure 4. The total insertion loss for the 23 mm long waveguides written 100 µm below the glass in aluminosilicate glass in given for the different pulse energies and writing speeds. The minimum insertion loss was obtained for a writing speed of 5 mm/s and pulse energy of 300 nJ.

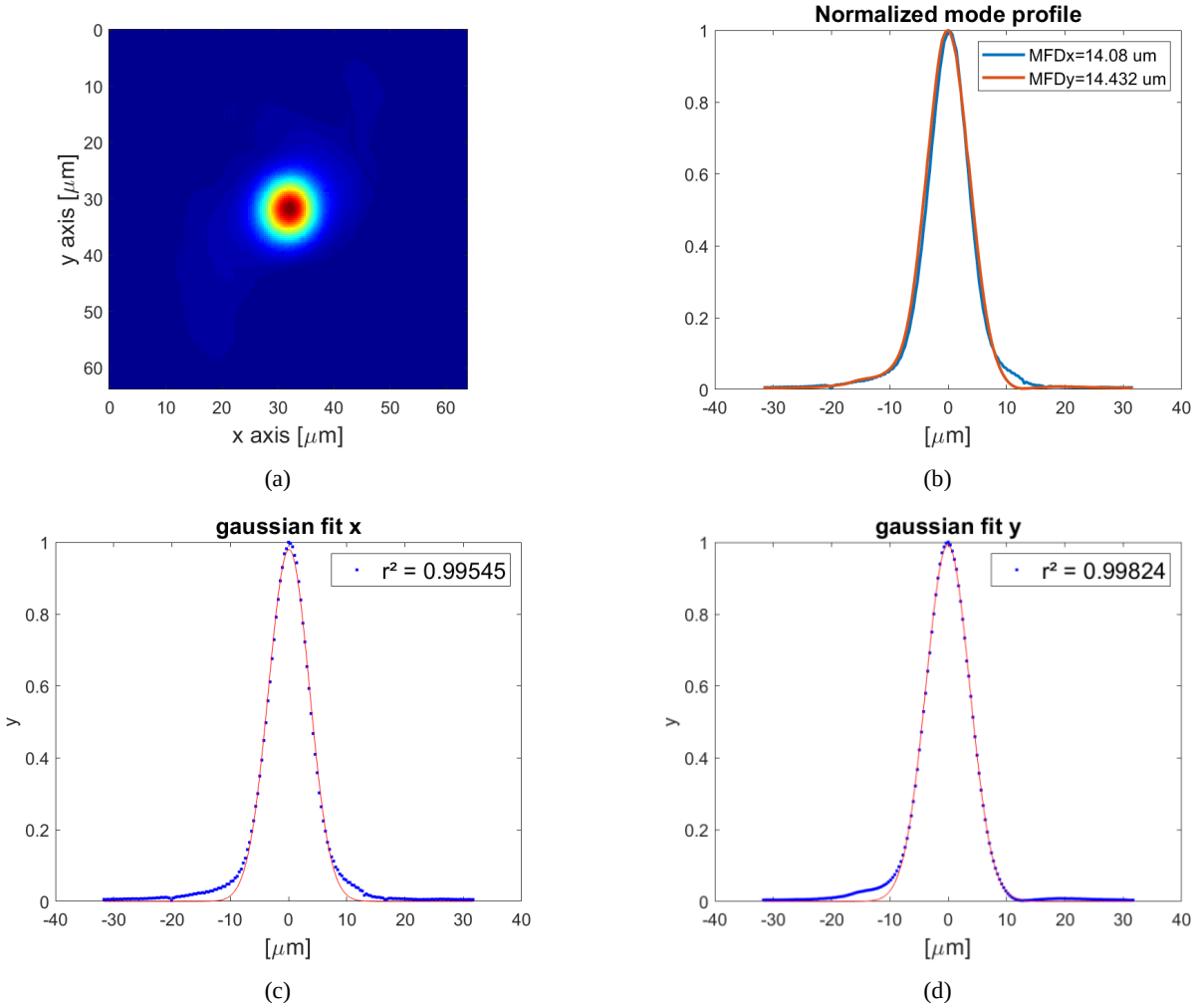

Figure 5: An example of the measured mode profile of a femtosecond laser written waveguide with writing speed equal to 5 mm/s and a pulse energy of 300 nJ written 100 µm below the glass surface. Figure (a) shows the mode profile as captured with the IR

camera at a wavelength of 1550 nm. Figure (b) shows the normalized cross-sections in x and y direction taken at the intensity spot. In (c) and (d) the fit with a gaussian curve is shown for both the x and y cross sections respectively.

3.2 Laser-written waveguide coupler

An example of a coupler with coupling length of 2.5 mm and 17 µm pitch, resulting in an almost 50:50 splitting ratio, is shown in Figure 6a. Figure 6b shows a cross section at the maximum intensity on the y-axis. Figure 7 shows the coupling ratios as a function of the coupling length and a comparison is made with the simulations. By tuning the coupling length between 1 and 4.5 cm, coupling ratios between 87:13 and 15:85 can be obtained. Note that compared to the simulations, the graph corresponding with the experimental data is scaled to shorter coupling lengths. In the simulations, the waveguides are modelled with a step index, while in reality, the waveguides do not have a step index profile, which can possibly explain this scaling. In addition, it is noted that 100% coupling cannot be obtained.

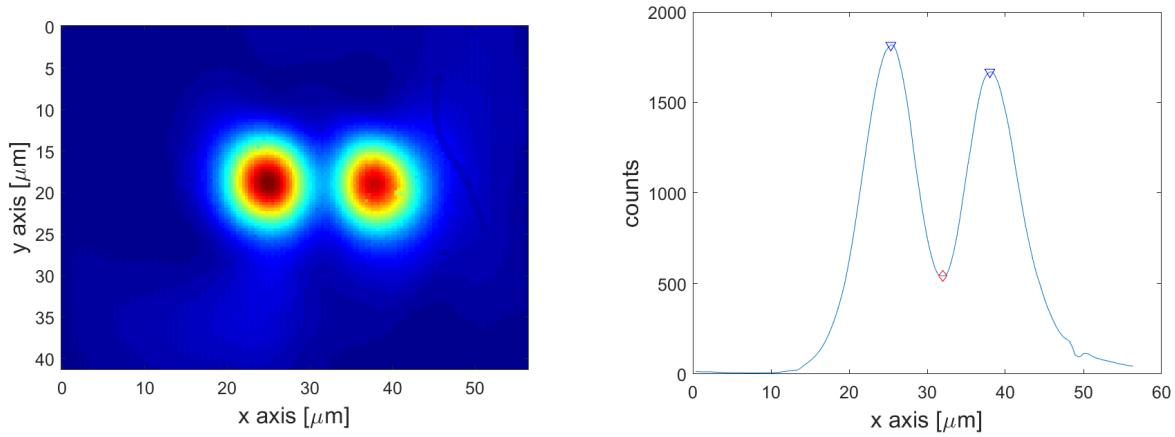

(a) (b)

Figure 6. Figure (a) shows the mode profiles as obtained with the IR camera of a coupler with pitch 17 µm and coupling length 2.5mm. The left spot corresponds to the in-coupling waveguide, while the right spot shows the out-coupling waveguide. Figure (b) shows the cross section taken at the position on the y axis where the maximum intensity was obtained.

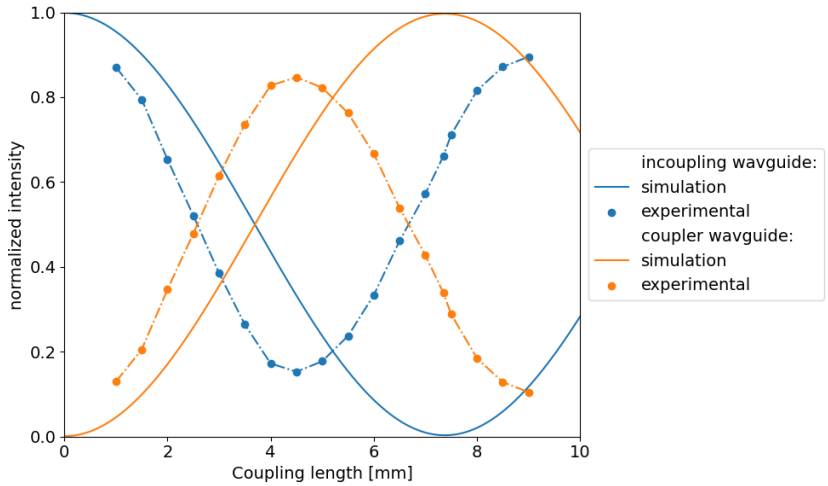

Figure 7. A comparison between the coupling ratios as obtained via the EME simulation in Lumerical and the measured ratios of the couplers with varying coupling length and with a pitch of 17 µm.

The second sample with coupling length of 6 mm, with intended 30:70 coupling ratio, and divergent waveguide showed 6.04 dB loss in the in-coupling waveguide and 12.72 dB loss in the coupler waveguide. The resulting coupling ratio is

82:18 which means the actual coupling length was around 8 mm. This was to be expected due to the low angle (1°) of the divergent waveguide, effectively extending the overlap length of both waveguides. Figure 8 shows the spots of 1550 nm light at the outcoupling side of the sample.

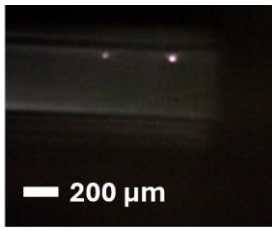

Figure 8. The figure shows the outcoupling side of the coupler sample with diverging waveguide. Two clear spots of 1550 nm light can be seen. The left spot is the coupling waveguide while the right spot is the light which remained in the in-coupling waveguide.

3.3 Laser written Bragg grating

The Bragg grating with the highest reflectivity achieved until now, equal to 5.93%, was obtained with pulse energy of 600 nJ, duty cycle equal to 10% and writing speed of 5 mm/s. The Bragg grating reflection spectrum is shown in Figure 9. Compared to the intended Bragg wavelength of 1550 nm, a blue shift of about 2 nm was observed for all parameter sets. Because the refractive index of the glass was used in the calculation of the grating period, the effective index was being underestimated and therefore a shift is caused in the Bragg wavelength.

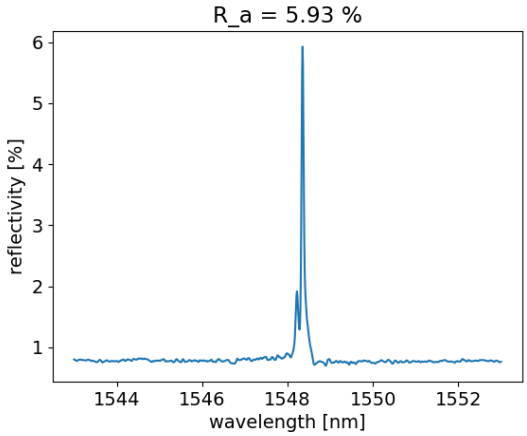

Figure 9. The reflection spectrum of the Bragg grating inscribed with a pulse energy of 600 nJ, a duty cycle of 10% and 5 mm/s writing speed. The total focused laser energy in 1 voxel equaled 31 µJ.

Duty cycles of 50% always resulted in very a low reflectivity (<0.75%). It is assumed that the contrast between voxels is not large enough due to the heat diffusion from the focal spot of the laser resulting in a modified zone which is larger than the focal spot [12].

When the total energy focused in the voxel (pulse energy x number of pulses in a voxel) exceeded 100 µJ, spectral broadening could be observed as is shown in figure 10. This was consistent for the 3 parameter sets where the total energy per voxel was 130, 130 and 156 µJ, whereas, for the Bragg grating spectrum shown in figure 9, only 31 µJ was focused in the voxel. Possible reasons could be multimode behaviour or non-uniformity of the voxels due to large modified zones as a result of the high energy focussed in the voxel.

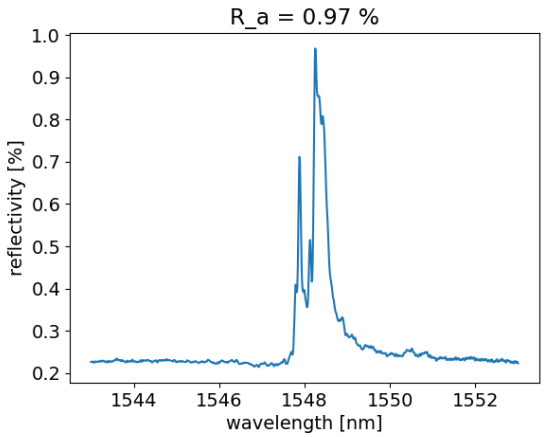

Figure 10. The reflection spectrum of the Bragg grating inscribed with a pulse energy of 500 nJ, a duty cycle of 25% and 0.25 mm/s writing speed, with noticeable spectral broadening. The total focused laser energy in 1 voxel equaled 130 µJ.

4. CONCLUSION

In this work the building blocks, i.e laser-written low-loss single mode waveguides, couplers and Bragg gratings, for an aluminosilicate glass based connector platform were studied. The platform should enable the connection of optical fibers which cannot be connected using conventional splicing or connector technology, such as in composite embedded optical fibers. Femtosecond laser technology was used to inscribe single mode waveguides in aluminosilicate glass. After optimizing the inscription parameters, waveguides with an estimated propagation loss of 0.65 dB/cm and slightly elliptical mode profile with MFDs of 13.77±0.91 and 15±1.53 were obtained. The coupling loss with standard SMF-28 fibers was estimated to be 0.53±0.15 dB. These waveguides were then used to design a tunable coupler by varying the coupling length from 1 to 4.5 cm. As such, the coupling ratio can be tuned between 87:13 and 15:85, respectively for a pitch of 17 µm. Lastly, first order Bragg gratings were inscribed using the pulse modulation technique. A parameter sweep was performed to obtain 23 mm long Bragg gratings with a maximum reflectivity of 5.9% in the C-band for the best parameter set.

ACKNOWLEDGEMENTS

These work received funding from the VLAIO Baekeland mandate (HBC.2020.2888).

REFERENCES

[1] Lamberti, A., Chiesura, G., Luyckx, G., Degrieck, J., Kaufmann, M., & Vanlanduit, S. (2015). Dynamic Strain Measurements on Automotive and Aeronautic Composite Components by Means of Embedded Fiber Bragg Grating Sensors. Sensors, 15(10), 27174-27200. doi:10.3390/s151027174

[2] Kara De Maeijer, P., Voet, E., Windels, J., Van den bergh, W., Vuye, C., & Braspenninckx, J. (2020). Fiber Bragg grating monitoring system for heavy-duty pavements.

[3] Juwet, T., Luyckx, G., Lamberti, A., Creemers, F., Voet, E., & Missinne, J. (2024). Monitoring of Composite Structures for Re-Usable Space Applications Using FBGs: The Influence of Low Earth Orbit Conditions. *Sensors, 24*(1). doi:10.3390/s24010306

[4] Jaiswal, P. R., Kumar, R. I., Juwet, T., Luyckx, G., Verhaeghe, C., & De Waele, W. (2023). Experimental deformation analysis of an adhesively bonded multi-material joint for marine applications. Strain, 59(2), e12433. doi:https://doi.org/10.1111/str.12433

[5] McKenzie, I., Ibrahim, S., Haddad, E., Abad, S., Hurni, A., & Cheng, L. K. (2021). Fiber Optic Sensing in Spacecraft Engineering: An Historical Perspective From the European Space Agency. Frontiers in Physics, 9. doi:10.3389/fphy.2021.719441
[6] Joe, H.-E., Yun, H., Jo, S.-H., Jun, M. B. G., & Min, B.-K. (2018). A review on optical fiber sensors for environmental monitoring. International Journal of Precision Engineering and Manufacturing-Green Technology, 5(1), 173-191. doi:10.1007/s40684-018-0017-6
[7] Presti, D. L., Massaroni, C., Leitão, C. S. J., Domingues, M. D. F., Sypabekova, M., Barrera, D., . . . Schena, E. (2020). Fiber Bragg Gratings for Medical Applications and Future Challenges: A Review. IEEE Access, 8, 156863-156888. doi:10.1109/ACCESS.2020.3019138
[8] Taffoni, F., Formica, D., Saccomandi, P., Pino, G. D., & Schena, E. (2013). Optical Fiber-Based MR-Compatible Sensors for Medical Applications: An Overview. Sensors, 13(10), 14105-14120. doi:10.3390/s131014105
[9] Van Hoe, B., Lee, G., Bosman, E., Missinne, J., Kalathimekkad, S., Maskery, O., Van Steenberge, G. (2012). Ultra Small Integrated Optical Fiber Sensing System. Sensors, 12(9), 12052-12069. doi:10.3390/s120912052
[10] Geudens, V., Nategh, S., Van Steenberge, G., Belis, J., & Missinne, J. (2024). Laser micromachined 3D glass photonics platform demonstrated by temperature compensated strain sensor. Optics & Laser Technology, 169, 109970. doi:https://doi.org/10.1016/j.optlastec.2023.109970
[11] Low, D. K. Y., Xie, H., Xiong, Z., & Lim, G. C. (2005). Femtosecond Laser Direct Writing of Embedded Optical Waveguides in Aluminosilicate Glass. Appl. Phys. A: Mater. Sci. Process, 81, 1633-1638. doi:10.1007/s00339-005-3324-z
[12] Miese, C., Withford, M. J., & Fuerbach, A. (2011). Femtosecond laser direct-writing of waveguide Bragg gratings in a quasi cumulative heating regime. Optics Express, 19(20), 19542-19550. doi:10.1364/OE.19.019542
[13] Spaleniak, I., Gross, S., Jovanovic, N., Williams, R. J., Lawrence, J. S., Ireland, M. J., & Withford, M. J. (2014). Multiband processing of multimode light: combining 3D photonic lanterns with waveguide Bragg gratings. Laser & Photonics Reviews, 8(1), L1-L5. doi:https://doi.org/10.1002/lpor.201300129
[14] Lapointe, J., Parent, F., Soares de Lima Filho, E., Loranger, S., & Kashyap, R. (2015). Toward the integration of optical sensors in smartphone screens using femtosecond laser writing. Optics Letters, 40(23), 5654-5657. doi:10.1364/OL.40.005654